GEOLOGY

Volcanic CO$_2$ tracks the incubation period of basaltic paroxysms

Alessandro Aiuppa[1]*, Marcello Bitetto[1], Dario Delle Donne[1,2,3], Francesco Paolo La Monica[1,3], Giancarlo Tamburello[4], Diego Coppola[5], Massimo Della Schiava[1,3], Lorenzo Innocenti[3], Giorgio Lacanna[3], Marco Laiolo[5], Francesco Massimetti[5], Marco Pistolesi[6], Maria Cristina Silengo[3], Maurizio Ripepe[3]

The ordinarily benign activity of basaltic volcanoes is periodically interrupted by violent paroxysmal explosions ranging in size from Hawaiian to Plinian in the most extreme examples. These paroxysms often occur suddenly and with limited or no precursors, leaving their causal mechanisms still incompletely understood. Two such events took place in summer 2019 at Stromboli, a volcano otherwise known for its persistent mild open-vent activity, resulting in one fatality and damage to infrastructure. Here, we use a post hoc analysis and reinterpretation of volcanic gas compositions and fluxes acquired at Stromboli to show that the two paroxysms were preceded by detectable escalations in volcanic plume CO$_2$ degassing weeks to months beforehand. Our results demonstrate that volcanic gas CO$_2$ is a key driver of explosions and that the preparatory periods ahead of explosions in basaltic systems can be captured by precursory CO$_2$ leakage from deeply stored mafic magma.

INTRODUCTION

The geological and historical records of volcanic activity at many basaltic volcanoes are punctuated by sudden but powerful paroxysmal explosions (1–7). These vigorous blasts abruptly interrupt the quiescent degassing and mildly explosive activity characteristic of basaltic volcanoes (5); the recent examples of Fuego in 2018 (7) and Merapi in 2010 (8), in particular, demonstrate the potential for widespread destruction and considerable loss of life.

The processes that govern fragmentation of low-viscosity basaltic magma have increasingly been targeted by volcanological research (1, 9–11), yet the trigger mechanisms that initiate such explosive eruptions remain poorly understood compared to those of silicic magmas (12, 13). However, petrological information (2, 14–17), geophysical observations (18), and models (9, 19) point to magma overpressure caused by outgassing of a CO$_2$-rich gas phase as a viable candidate. Basaltic magmas are often CO$_2$ rich (20) and, because of the limited CO$_2$ solubility in silicate melts, are often saturated with a CO$_2$-rich gas phase in mid- to deep-crustal reservoirs (2, 19, 21). As magma reservoirs are resupplied with gas-rich mafic melt ascending from depth before eruption, upward migration of exsolved CO$_2$-rich volatiles in low-viscosity stored magma leads to foam accumulation at reservoirs' roofs, causing pressure buildup and, ultimately, driving magma to erupt violently (22, 23). Degassing of magma in the shallow conduit has also been invoked as a top-down mechanism that triggers eruption of mafic magma (24).

The strong causal implication of CO$_2$-rich gas as an eruption trigger has motivated research into volcanic CO$_2$ release through summit vents, fumaroles, and volcano flanks (25). Instrumented volcanic gas plume monitoring (26–29), in particular, has been central to confirming a role for CO$_2$ in driving explosive basaltic volcanism

(30, 31). In the few localities where permanent gas plume networks have been established, an escalation of CO$_2$ fluxes and CO$_2$/SO$_2$ ratios has been observed before eruption, such as before lava fountaining at Etna (18, 32), paroxysmal activity at Villarrica (27), and violent explosive sequences at Turrialba (28) and Poás (29). The Merapi 2010 centennial (Plinian) eruption was also preceded by CO$_2$/SO$_2$ ratio increases in the discontinuously sampled dome fumaroles (8). However, only <20 volcanoes are instrumented with permanent gas monitoring networks at the time of writing (25). This, combined with the rapid (days) (33, 34) time scales of final preeruptive mafic magma ascent, and the difficulties in identifying the subtle changes that should accompany the progressive pressure buildup at depth in the months/years beforehand (21) have limited our ability to use volcanic gases to issue eruption warnings and to fully understand the processes occurring in the run-up to the events.

Some of the most frequent basaltic paroxysmal explosions are observed at Stromboli volcano (Southern Italy). These violent (volcanic explosivity index = 3) "paroxysms" interrupt the "regular" persistent mild (Strombolian) activity at typical recurrence times of one to two events per decade (35, 36). Paroxysms are typically sudden and short lived (duration, <600 s) and form high (3 to 8 km) eruptive plumes (35). These eruptive plumes produce a variety of hazardous phenomena, including fallout of hot coarse ballistics over the island's inhabited coastal sectors and the emplacement of tsunamigenic pyroclastic density currents along the shores (37). Thus, paroxysmal events pose a substantial hazard for inhabitants, scientists, and visitors (36).

In addition to having a well-developed monitoring network (18, 26), Stromboli is an ideal case study to investigate the triggering mechanisms for basaltic paroxysms as two distinct process models have been identified. The two explosions of 5 April 2003 (38, 39) and 15 March 2007 (40), the first paroxysmal eruptions since the introduction of comprehensive monitoring infrastructure at the volcano, occurred during lateral effusive phases. A top-down (effusive) trigger mechanism for these paroxysms has been proposed based on empirical observations and modeling, whereby drainage of upper conduit magma into the developing lava flow field drives decompression of

[1]Dipartimento di Scienze della Terra e del Mare, Università di Palermo, Palermo, Italy. [2]Istituto Nazionale di Geofisica e Vulcanologia, Osservatorio Vesuviano, Napoli, Italy. [3]Dipartimento di Scienze della Terra, Università di Firenze, Firenze, Italy. [4]Istituto Nazionale di Geofisica e Vulcanologia, Sezione di Bologna, Bologna, Italy. [5]Dipartimento di Scienze della Terra, Università di Torino, Torino, Italy. [6]Dipartimento di Scienze della Terra, Università di Pisa, Pisa, Italy.
*Corresponding author. Email: alessandro.aiuppa@unipa.it

deeply stored (7 to 10 km deep) (*41*) crystal-poor [low porphiricity (LP)] magma (*26*, *42*–*44*). In contrast, unlike the 2003 and 2007 events, several historical paroxysms [e.g., the 1930 event; (*37*)] have occurred during regular Strombolian activity, e.g., in the absence of an ongoing effusive phase. Instead, these events have been interpreted as the result of a bottom-up mechanism by which the addition of gas and mafic melt to the LP deep magma storage zone (*15*, *16*, *41*) causes pressurization, followed by rapid ascent and eruption (*45*). The absence of effusion trigger for this class of events implies no direct link with the shallow volcanic system driving regular activity.

The first of such deep-triggered paroxysms to be captured by monitoring instrumentation occurred at Stromboli on 3 July 2019. This event was followed by lava effusion (July 3 to August 31) and, subsequently, by a second paroxysm on 28 August 2019 (*18*, *46*). The summer 2019 eruptive crises thus present a unique opportunity to study two closely spaced events with apparently contrasting (bottom-up versus top-down) source mechanisms. The paroxysm on 3 July 2019 was not preceded by any noticeable precursory change in surface volcanic activity (*47*) and, since ground inflation anticipated the event by only 10 min (*18*), no alert warning was issued. Although real-time early-warning systems based on tiltmeter measurements have now been installed on Stromboli (*18*), identifying midterm precursors to paroxysms is urgently needed.

Here, we report on a detailed post hoc analysis and reinterpretation of volcanic gas records acquired during a 2.5-year period (May 2018 to December 2020) encompassing the July to August 2019 unrest. We demonstrate the utility of instrumental gas monitoring to track the precursory release of CO_2-rich gas from soon-to-erupt deeply rising magma. Our results have important implications for the understanding of the incubation periods before basaltic eruptions and for the role of magmatic gas in driving explosive activity.

RESULTS

The summer 2019 paroxysms

The paroxysmal explosion on 3 July 2019 started at 14:45:42 UTC. Although not preceded by any evident change in eruptive behavior (regular Strombolian activity level continued until the blast), ground inflation of ~14 μrad occurred over a period of ~10 min immediately before the event (*18*). The explosion generated a ~8-km-high eruptive column in a few tens of seconds (Fig. 1A), which produced dense tephra fallout (ash, lapilli, and bombs) over the island of Stromboli. The fallout phase lasted ~40 to 50 min and was particularly intense in the village of Ginostra (see Fig. 1), where one casualty was reported. Larger bombs and blocks ignited fires on impact with dry vegetation. Two pyroclastic flows were also generated inside the Sciara del Fuoco (Fig. 1) due to the partial collapse of the eruptive column; these flows produced a ~2-m-high tsunami as they entered the sea (*48*). The July 3 paroxysm caused substantial morphological changes to the crater terrace, with the accumulation of ~1 m of bombs and lapilli on the ground and the opening of a major collapse scar in the southwestern rim of the crater terrace (Fig. 1B). This scar enabled magma drainage from the upper conduit into the Sciara del Fuoco (Fig. 1B), feeding a lava flow that eventually reached the shore line. This effusive activity persisted, accompanied by vigorous explosive activity at the summit craters, until August 28 when (at 10:17:15 UTC) a second paroxysm took place (Fig. 1C). Although slightly smaller in scale than the first 2019 event (eruptive column of ~6 km), this second paroxysm also generated widespread tephra fallout,

particularly in the village of Stromboli, as well as a second tsunami-genic pyroclastic flow inside the Sciara del Fuoco. After the 28 August paroxysm, volcanic activity slowly declined in intensity (i.e., frequency and magnitude of Strombolian explosions), and effusive activity ceased entirely on 31 August 2019. Regular Strombolian activity continues until the time of writing.

Regular Strombolian activity between May 2018 and December 2020 was punctuated by seven major explosions (18 August 2018; 25 June 2019; 29 August 2019; 19 July 2020; and 10, 16, and 21 November 2020) (Fig. 2). These events are intermediate in size between regular and paroxysmal explosions in terms of column heights and erupted volumes (*35*), and their wide ballistic dispersal areas pose a potential hazard to local communities and visitors during the most extreme events (*36*). Tilt measurements (*18*) indicate that major explosions share similar (scale-invariant) conduit dynamics with regular and paroxysmal explosions. Five brief lava overflow events from the summit craters also occurred on 6 December 2018, 28 March, 31 March, 14 April, and 16 April 2020 (Fig. 2).

Volcanic gas plume composition

We characterize the composition of the volcanic gas plume emitted from the crater vents based on in situ measurements of in-plume CO_2 and SO_2 concentrations (Fig. 2) obtained using a fully autonomous multicomponent gas analyzer system (Multi-GAS; see Materials and Methods) (*21*). The observational period spans from 10 May 2018 (the Multi-GAS deployment day) to 31 December 2020, during which Multi-GAS operations are continuous. Data gaps are typically limited to only a few days at most (Fig. 2), with the exception of longer gaps during (i) 9 April to 15 June 2019 (due to instrument malfunctioning) and (ii) 4 to 21 July 2019 (since the July 3 eruption destroyed the instrument, which was replaced on July 22) (Fig. 2).

Our compositional time series, illustrated in Fig. 2, is obtained from postprocessing of the Multi-GAS dataset using an algorithm (see Materials and Methods) that identifies periods of temporal coherence in the CO_2 and SO_2 concentration time series (Fig. 3). Selecting periods of elevated CO_2 versus SO_2 correlation (Fig. 3C), we derive a temporal record of both concentrations and CO_2/SO_2 ratios (Fig. 2).

The top and middle panels in Fig. 2 highlight the temporal fluctuations of SO_2 and CO_2 concentrations during May 2018 to December 2020, as expressed in the form of (7 days averaged) frequency distributions of gas concentrations observed during each measurement interval (see Materials and Methods and Fig. 3). Averaging over 7-day intervals reduces high frequency variability due to changes in the wind field and other nonvolcanic phenomena (that occur over shorter time scales), thus rendering our concentration time series as more representative proxies for long-term changes in CO_2 and SO_2 degassing regimes, as found elsewhere (*49*, *50*). Figure 2 thus conveys information on the temporal fluctuations in both (i) the dominant (median) concentration levels (dark red color tones) and (ii) the normalized spread of gas concentrations around the median [light blue color tones correspond to frequency bins in which measurement occurrence frequency is 30 to 60% lower than the most frequent measurement bin (dark red)].

Our results evidence relatively stable SO_2 concentrations during the 2.5-year measurement interval. The median SO_2 concentrations typically maintain at ~2 to 3 ppmv, with periodic intervals in which they increase to ~5 to 10 ppmv. Maximum SO_2 concentrations rarely exceed 20 ppmv. Overall, no obvious temporal trend is observed, with
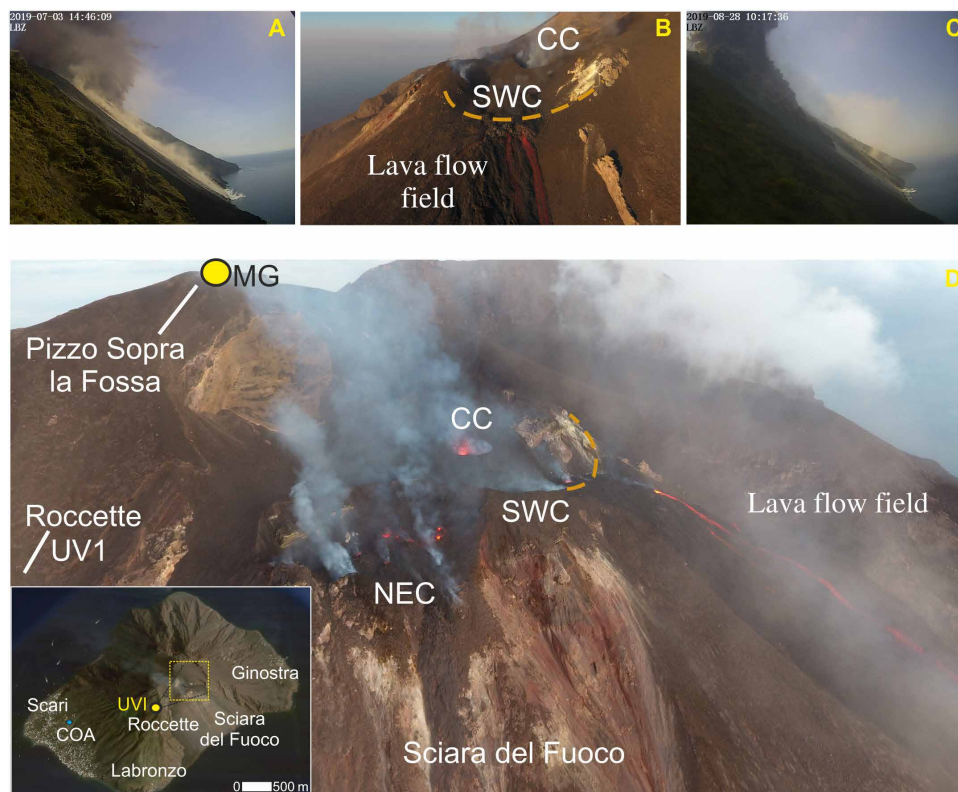
Fig. 1. Stromboli volcano in 2019 and its volcanic gas network. (**A**) The onset phases of the 3 July 2019 paroxysm (*18*), taken by the LGS (Laboratorio Geofisica Sperimentale, Università di Firenze) webcam located at the Labronzo site [see inset of (D)]. (**B**) An aerial view of the southwestern portion of the crater terrace (taken on 26 July 2019 using a DJI phantom 4 drone), showing the upper portion of the 2019 lava flow field issuing from an effusive vent on the scar (orange dashed line) left by collapse of the western crater's outer rim on July 3. The southwest (SWC) and central (CC) craters are indicated. (**C**) The onset phases of the 28 August paroxysm, same view and webcam as in (A). (**D**) Aerial view of Stromboli's summit on 26 July 2019 (using a DJI phantom 4 drone) showing the crater terrace (NEC, northeast crater), and the Pizzo Sopra la Fossa where the Multi-GAS (MG) operates. The lava flow field inside the Sciara del Fuoco is also visible on the right. Inset: Google Earth map of Stromboli island, showing the localities mentioned in the main text and the Roccette site where the UV1 camera system is deployed. The black dashed lines identify the camera field of view, while the yellow box identifies the area imaged by the aerial photo in (D).

the exception of a ~4-month period (September to December 2019) following the summer 2019 effusive phase during which both median and maximum SO_2 concentrations remain persistently low. This phase is concomitant with an overall decline in SO_2 fluxes (see Fig. 4A and Discussion below), suggesting that shallow degassing was suppressed following the extensive summer 2019 effusion.

Atmospheric background-corrected CO_2 concentrations (Fig. 2B) exhibit clear temporal trends. We find that the median background-corrected CO_2 concentrations systematically and monotonically increase from summer-fall 2018 (<50 ppmv) to June to early July 2019, when they exceed 100 ppmv in the days before the 3 July paroxysm. During the effusive eruption, CO_2 concentrations remain stable at ~50 ppmv (SO_2 concentrations are similarly above background at ~10 ppmv). After effusion, the median background-corrected CO_2 concentrations remain ≤50 ppmv but then begin to increase again in May 2020, reaching a peak immediately before a major explosion on 19 July 2020. After this event, and until the end of 2020, the median background-corrected CO_2 concentrations remain elevated (~50 ppmv) relative to previous values earlier in the year.

Combined processing of SO_2 and CO_2 concentration time series (Fig. 3 and Materials and Methods) yield molar CO_2/SO_2 ratios in the emitted gas plume (Fig. 2C). Large fluctuations in gas composition

occur between 2018 and 2020. The median CO_2/SO_2 ratios (dark red color tones) remain ≤10 to 15 during 2018. However, from late January 2019 onwards, these ratios increase to ~20, and this CO_2-rich phase persists until April 2019. Further elevated mean CO_2/SO_2 ratios peak at 20 to 30 in late June to early July, following a 2-month gap in the time series (due to instrumental failure). Notably, the period immediately before the 3 July event is characterized by a distinctive bimodality in CO_2/SO_2 ratios; here, CO_2/SO_2 ratios of 20 to 30 coexist with a secondary peak in ratios < 10. During the 2019 effusive phase, the CO_2/SO_2 ratios are initially low (median = ~5) but then increase before and following the August 28 paroxysm. After effusion, CO_2/SO_2 ratios fluctuate at high values (median = 10 to 30) until January 2020; however, in this case, the high ratio reflects low SO_2 abundances (Fig. 2A) rather than high CO_2 abundances (Fig. 2B). Throughout most of 2020, the median CO_2/SO_2 ratio remains stable at ~5 but peaks again in the weeks before the major explosions of 19 July 2020 and 10 November 2020.

SO_2 and CO_2 fluxes

We derive volcanic SO_2 fluxes from ultraviolet (UV) camera measurements (see Materials and Methods; red tones in Fig. 4A). During the 2.5-year measurement period, the SO_2 flux is highly variable with a mean average of 97 ± 64 (σ) tons/day. During the
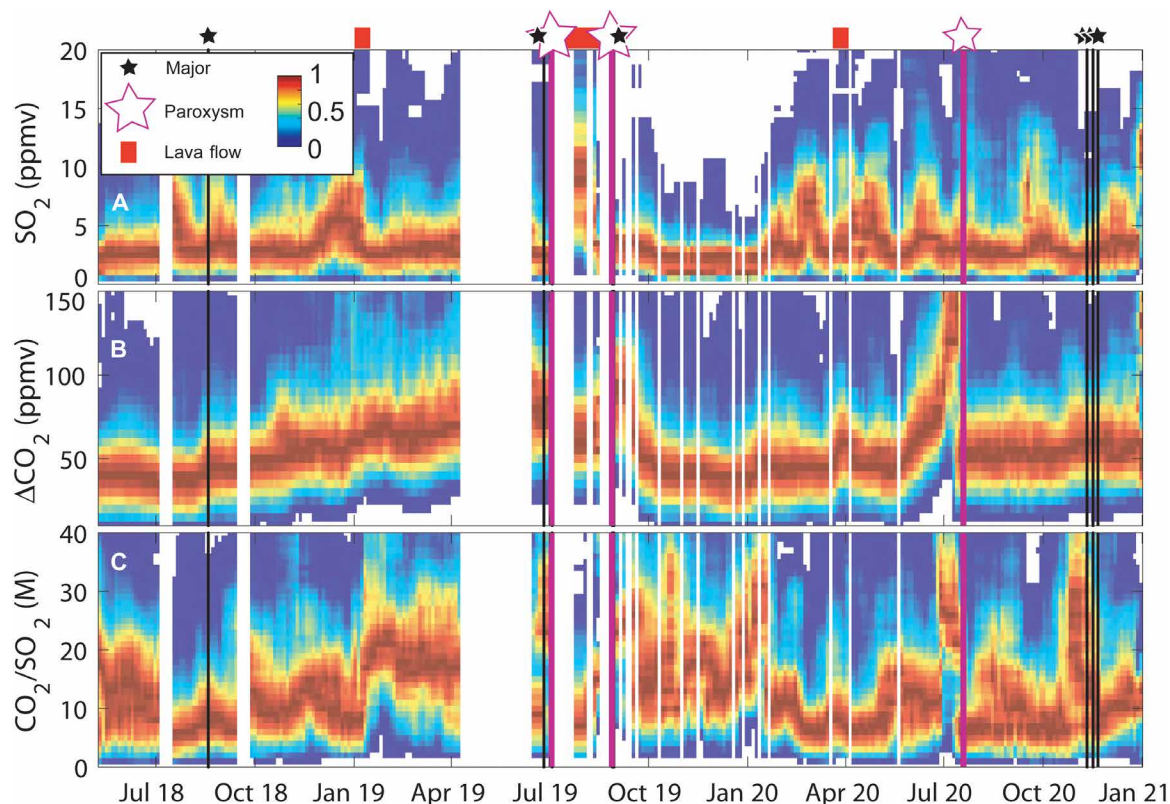
Fig. 2. Volcanic gas plume compositions. Time series of (**A**) plume SO_2 concentrations [in parts per million by volume (ppmv)], (**B**) plume CO_2 concentrations (in ppmv), and (**C**) plume CO_2/SO_2 (molar) ratios. In (B), the CO_2 concentrations are presented as corrected for atmospheric background (ΔCO_2; above atmospheric background). Results are displayed as 7-day averaged normalized distributions of all measurement intervals satisfying two correlation criteria (SO_2 concentration greater than 1 ppmv and Pearson correlation coefficient between SO_2 and CO_2 concentrations greater than 0.9 within a 60-s moving window; see Materials and Methods and Fig. 3). Vertical bars with stars identify paroxysmal and major explosions [the 19 July 2020 event is interpreted as intermediate in size between major explosions and paroxysms, based on deformation records (18)]. Red horizontal bars are for lava effusions. SO_2 plume concentrations are generally stable within 0 to 5 ppmv with periodic month-lived increases. Background-corrected CO_2 plume concentrations exhibit a steady increasing trend from late-2018 to mid-2019, culminating shortly before the 3 July paroxysmal eruption. They then decrease to ~40 ppmv after the summer 2019 unrest. A significant and fast increasing trend is detected in the 2 months before a large major explosion occurred on 19 July 2020. CO_2/SO_2 molar ratios also peak in the week before the 3 July paroxysmal eruption and remain at generally high levels throughout 2019. Fast CO_2/SO_2 ratio increases are detected in the weeks before the July and November 2020 major explosions.

summer 2019 effusive phase, the SO_2 flux is a factor ~3 higher [mean, 272 ± 95 (σ) tons/day], and the maximum SO_2 flux (of 475 tons/day) is consistently measured (on 14 August 2019). High SO_2 emission rates are typical of Stromboli's effusive eruptions and reflect more efficient magma convection in the shallow upper conduits (*51, 52*). The SO_2 flux decreases in September 2019 following cessation of lava effusion on 30 August, reaching pre-effusion levels by October 2019.

We calculate the volcanic CO_2 flux by combining daily CO_2/SO_2 ratios (Fig. 2C) with the corresponding daily-averaged SO_2 flux (Fig. 4A). The derived CO_2 flux (in tons/day) temporal record is illustrated in Fig. 4B, and a detail of the summer 2019 effusive crisis is offered in Fig. 5. To fill gaps in the time series resulting from unfavorable wind directions or equipment malfunction, we linearly interpolate the CO_2/SO_2 ratio based on the measured values of each side of the hiatus (of Fig. 2C). As the CO_2 flux results for 9 April to 15 June 2019 and 2 to 21 July 2019 are based entirely on interpolated CO_2/SO_2 ratios (and measured SO_2 fluxes), they should be considered with caution as the linear interpolation may mask short-term variability. However, the continuous long-term increasing trend in CO_2 plume concentrations (Fig. 2B), together with the slight increase

in SO_2 flux (Fig. 4A) during the data gap, suggests that a linear interpolation is robust.

We find that the two paroxysmal explosions in 2019 are both preceded by median daily CO_2 fluxes (dark red tones) of ~4000 tons/day (Figs. 4B and 5), substantially greater than the background CO_2 flux of ≤1000 tons/day, characteristic of regular Strombolian activity (e.g., during 2018 and 2020). Similar to the pattern observed in CO_2/SO_2 molar ratios, the CO_2 flux peaks at a maximum of ~10,000 tons/day before both paroxysms, a factor of 3 to 5 higher than the peak CO_2 emissions during regular activity (Figs. 4B and 5).

DISCUSSION
CO_2 escalates before basaltic paroxysms
The limited solubility of CO_2 in silicate melts results in deep exsolution of a CO_2-rich magmatic fluid phase from ascending mafic melts (*2, 19, 20*). Overpressurization of a deep magma reservoir is therefore likely driven by a fluid phase composed predominantly of CO_2 (*22, 23*). At Stromboli, there is abundant petrological evidence indicating that paroxysms originate from deep (7 to 10 km depth) in the volcano's plumbing system (*14–16*). Although various trigger
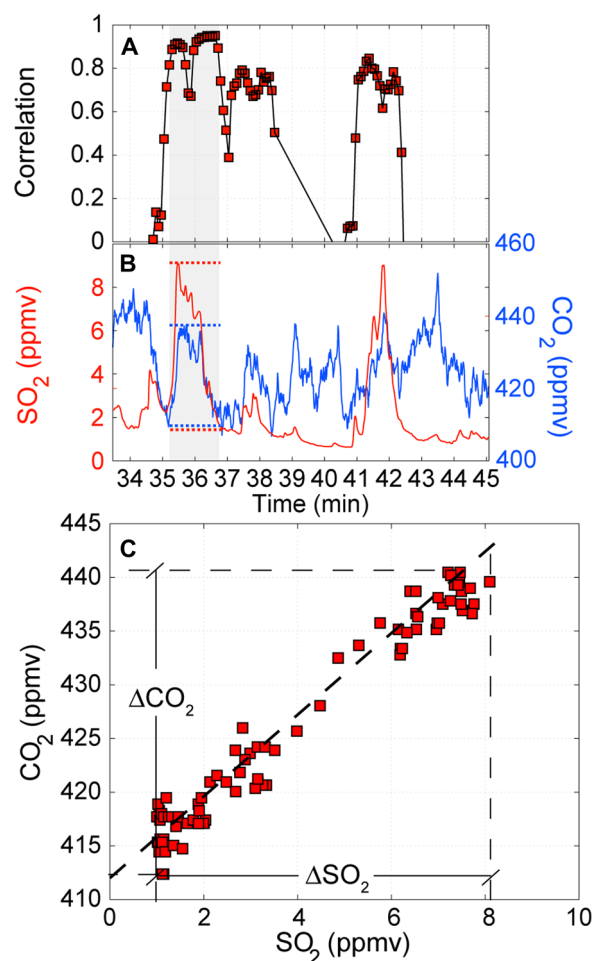
Fig. 3. Data processing. (**A**) Example of correlation analysis adopted for the detection of coherent SO_2 and CO_2 concentration time windows within the raw Multi-GAS time series. CO_2 and SO_2 concentration records (**B**) show repetitive 50- to 100-s-long pulses associated with volcanic plume fumigation at the Multi-GAS site. A CO_2/SO_2 ratio is calculated (from the slope of the best-fit regression in a SO_2 versus CO_2 space) (**C**) only for those data segments showing Pearson correlation coefficient (A) greater than 0.9 (gray-colored area in figure). CO_2 and SO_2 concentration intensities (plotted in Fig. 2, A and B) are taken as their maximum variation within the selected window (maximum to minimum intensities).

mechanisms have been proposed (*14–16, 19, 21, 41–43*), there is general consensus that paroxysms themselves are caused by fast ascent and injection of a deeply stored, gas-rich LP magma into the shallow plumbing system (*16*).

This deep trigger has motivated research on volcanic CO_2, as available volatile saturation models predict that a CO_2-dominated gas phase (with high CO_2/SO_2 ratios) coexists in equilibrium with the LP magma at reservoir conditions and during deep ascent (*53*). In contrast, the degassed high-porphiricity (HP) magma residing in the upper conduits—and which feeds regular activity—is CO_2 poor and in equilibrium with a gas phase with low CO_2/SO_2 ratio (*53*). Correspondingly, a precursory escalation in CO_2 gas release is predicted by models during decompressional degassing of the LP magma before large explosions. These model expectations found first observational evidence before the March 2007 paroxysm (*26*).

We have presented several lines of evidence that support an escalation in CO_2 degassing before the 2019 paroxysms: (i) The in-plume CO_2 concentrations gradually increase throughout late 2018 to early July 2019 and peak in weeks before the 3 July paroxysm (Fig. 2B). (ii) The CO_2/SO_2 ratio (Fig. 2C) increases since late January 2019 to peak before the 3 July 2019 paroxysm, and such CO_2-rich compositions persist until January 2020, months after the termination of lava effusion in 31 August 2019. Notably, the bimodality in measured CO_2/SO_2 ratios before the 3 July paroxysm (Fig. 2C) suggests that the magmatic volatile phase potentially includes contributions from both shallow- and deep-derived gas during the final ascent of the LP magma before the blast.

The fluctuations in plume CO_2/SO_2 ratios at Stromboli reflect temporal changes in the relative gas contributions from the deep (CO_2-rich) and shallow (CO_2-poor and SO_2-rich) magma storage zones (*53*). Hence, a high CO_2/SO_2 ratio does not necessarily imply an elevated deep gas flux and, instead, can also derive from a reduced level of shallow magma degassing. For example, we propose that a reduced SO_2 contribution from shallow conduit magma is likely to have caused the ~4-month-long (September to December 2019) period of high CO_2/SO_2 ratios following the 2019 unrest, as supported by concurrent stable, low SO_2 concentrations (Fig. 2A) and declining SO_2 fluxes (Fig. 4A).

To unequivocally identify periods associated with heightened deep CO_2 release, we rely on our CO_2 flux record (Figs. 4B and 5). This time series highlights, unambiguously, that a surge of deep CO_2 gas is associated with Stromboli's unrest during summer 2019, with daily CO_2 fluxes peaking at a factor of ~4 above typical background values (<1000 tons/day) before both blasts. Our results provide compelling evidence that volcanic CO_2 flux is an effective tracer of deep degassing, thus supporting previous work at Etna (*21, 32, 54*), Villarrica (*27*), Turrialba (*28*), and Poás (*29*), where elevated fluxes of deep-derived volatiles have been shown to precede paroxysmal eruptions of basaltic magma (*25*).

Bottom-up eruption dynamics
Our preparoxysm CO_2 emissions can be used to test current models for the triggers of basaltic paroxysms. As magma differentiation and second boiling (*12*) are intrinsically excluded as triggers for basaltic paroxysms, one commonly invoked mechanism is magma reservoir overpressuring led by injection of gas and/or gas-rich melt from depth (*22, 23*). Such recharge events can be reconstructed from postevent analysis of the textural properties and chemical zonation of minerals in erupted pyroclasts (*17, 33, 34*). Taking the 3 July 2019 paroxysm at Stromboli as an example, modeling of Mg-Fe zoning profiles recorded in olivine crystals from pumices (*16*) suggests that the eruption was triggered by replenishment of the deep LP magma storage zone with a CO_2-rich gas phase. Notably, in contrast with some other larger-scale historical eruptions, little or no evidence was found for the addition of fresh basaltic magma to the LP magma storage zone, suggesting a dominant role for gas in eruption triggering (*16*). Elsewhere, petrological evidence suggests similarly that variations in the frequency and magnitude of recent paroxysmal eruptions at Volcan de Fuego, Guatemala—another open-vent magmatic system—can be explained by changes in the supply of deep-derived gas without the need to invoke the repeated transfer of new magma to shallow levels (*55*).

Our gas observations here are consistent with this mechanism, as the precursory escalation in CO_2 release before the 3 July 2019
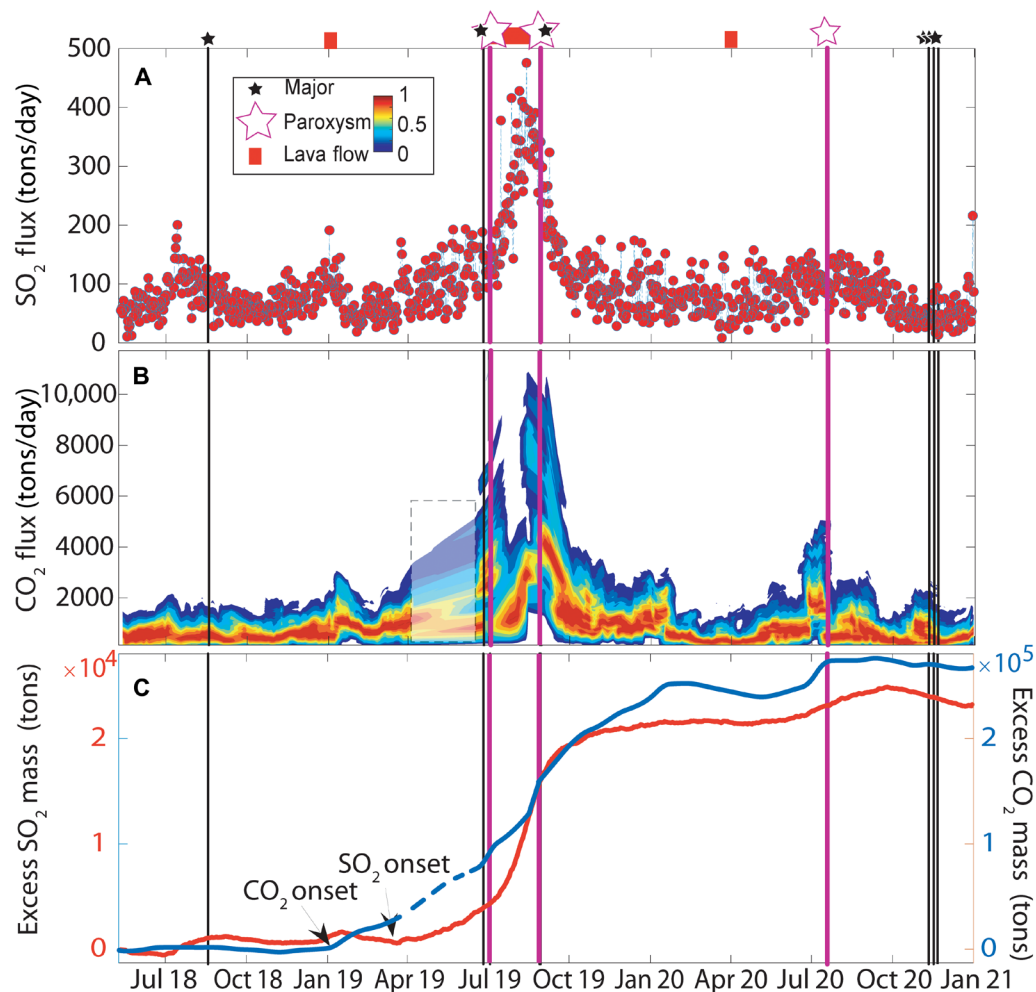
Fig. 4. Gas fluxes from the Stromboli's plume. Temporal record of daily averaged (**A**) SO_2 fluxes and (**B**) CO_2 fluxes. Data in (B) are calculated by multiplying the daily CO_2/SO_2 ratio frequency diagrams of Fig. 2C by the SO_2 fluxes of (A). Uncertainty in the derived CO_2 fluxes is evaluated at ≤40% from propagation of CO_2/SO_2 and SO_2 flux uncertainties. Gaps in the dataset (due to days of unsuccessful CO_2/SO_2 ratio determination because of the absence of plume fumigation at the Multi-GAS measurement site or Multi-GAS malfunctioning/failure) are filled by multiplying the measured SO_2 fluxes by CO_2/SO_2 ratios obtained from linear interpolation of the ratio time series (of Fig. 2C). These gaps are typically of a few days at most. Exceptions are the 9 April to 15 June 2019 [dashed area in (B)] and 4 to 21 July periods, in which the CO_2 flux results are based on data interpolation and should therefore be considered with caution. (**C**) Cumulative excess SO_2 (red) and CO_2 (blue) masses for the period from 10 May 2018 to 31 December 2020. The cumulative excess masses (see the main text) are obtained by subtracting from the measured (A) and calculated (B) fluxes the pre-unrest phase (May to December 2018) time-averaged fluxes of 71 and 500 tons/day, respectively. Interpolated trends are identified by dashed lines. This plot suggests that accelerating CO_2 degassing regime is likely to have started in early 2019. Visible accelerations in the excess CO_2 are seen before both paroxysms.

event is a strong indication for enhanced fluxing of Stromboli's plumbing system by CO_2-rich gas (Fig. 6A). The timing and duration of the CO_2 pulse before 3 July can be used to gain information regarding the time scales for an exsolved volatile phase to pressurize the magma reservoir sufficiently to force magma to ascend and finally erupt (Fig. 6B) (*22*, *23*). Constraining the timing of the onset of increasing CO_2 emissions is complicated by the gap in Multi-GAS data between 9 April and 15 June 2019. However, we use the linearly interpolated flux time series (Fig. 4B) to quantify the cumulative (May 2018 to December 2020) excess CO_2 mass release, illustrated (alongside the corresponding cumulative SO_2 mass) in Fig. 4C. We determine this excess mass by subtracting the time-averaged CO_2 flux (500 tons/day) for May to December 2018, which we consider representative of regular (pre-unrest) activity, from the cumulative time series. From this, we derive the cumulative excess mass

(Fig. 4C), which suggests that CO_2 degassing is likely to have started increasing between January and April 2019 (i.e., up to ~180 days before the 3 July 2019 blast; Figs. 6A and 7).

Overall, our results suggest a perturbation to Stromboli's deep plumbing system (e.g., degassing CO_2 at a higher rate than usual) months in advance of the 3 July paroxysm. This conclusion agrees with earlier results (*56*), showing that diffuse CO_2 degassing from soils in the Pizzo Sopra la Fossa area nearly doubled from December 2018 (~5000 $g \cdot m^{-2} \cdot day^{-1}$) to early July 2019 (~10,000 $g \cdot m^{-2} \cdot day^{-1}$), again suggesting escalating transport of deep-derived CO_2. Further, the several month-long incubation time scales for the 3 July paroxysm suggested by our data match well to the duration of precursory geochemical changes, as derived from mineral chronometers (*16*). These observations, especially Mg-Fe diffusion profiles in olivine crystals from the July 2019 pumices (*16*), indicate that increased
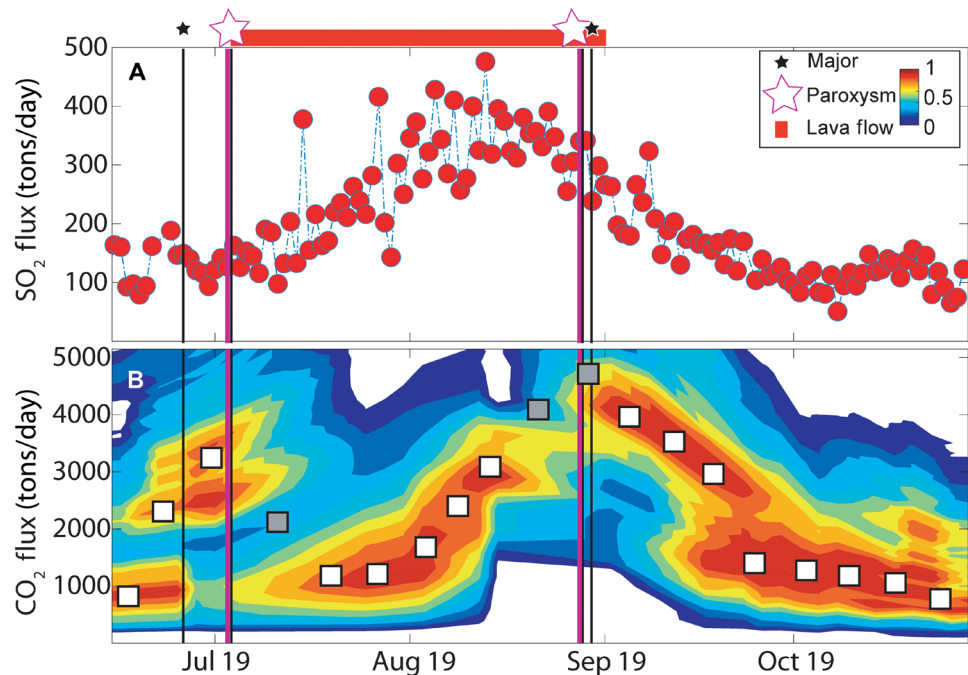
Fig. 5. A zoom of gas flux observations encompassing the summer 2019 effusive unrest. (**A**) SO_2 fluxes and (**B**) CO_2 fluxes. Squares in (B) identify weekly averaged median CO_2 fluxes (gray squares are for weeks in which no successful Multi-GAS measurements are available, and data interpolation was applied). The figure demonstrates two distinct CO_2 peaks before the two paroxysms. During the effusive event, a temporal lag is observed between SO_2 and CO_2 peaks. The 2019 effusive unrest thus involves (i) an initial period (3 July to 13 August) of rapid, efficient magma circulation in the upper conduits (high SO_2) and high lava output (*67*), followed by (ii) a second period (14 to 30 August) of vanishing shallow magma transport (declining SO_2 and magma effusion rates) [this study and (*67*)] but accelerating deep CO_2 degassing. Rapid drainage of conduit magma during 3 July to 13 August is thus a very likely causal factor for the 28 August paroxysm.
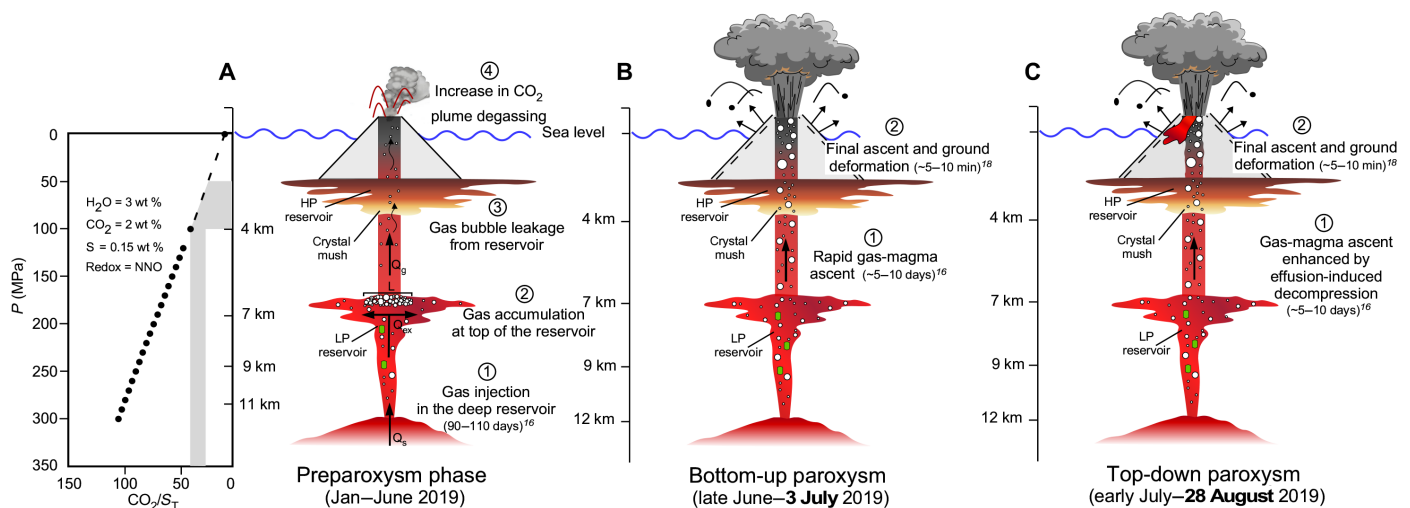

Fig. 6. A schematic graphical model for the triggers of basaltic paroxysms. (**A**) The pre–July 3 Stromboli paroxysm incubation period. Injection of CO_2-rich gas bubbles in the 7- to 10-km LP magma storage zone (*16*) leads to gas bubble accumulation on top of the reservoir's roofs and pressure build up. Q_s and Q_{ex} are, respectively, the supply rate of deeply rising bubbly magma and magma exchange rate from the feeder conduit into the sill (*60*). Passive gas leakage (Q_g) from the developing bubble cap (of length L) leads to escalating CO_2 fluxes in the crater plume starting from ~180 days before the 3 July 2019 blast. The inset on the left shows the pressure dependence on the magmatic gas CO_2/S_T (S_T = total sulfur), derived (*53*) from using a saturation model initialized at conditions relevant to Stromboli [H_2O = 3 weight % (wt %); CO_2 = 2 wt %; S = 0.15 wt %; redox conditions at the nickel-nickel oxide (NNO) buffer]. The high plume CO_2/SO_2 ratios measured before 3 July 2019 (Fig. 2C) imply minimum gas source depth of 2.5 to 4 km below the summit (see gray-filled area); these are minimum source depths because deeply rising gas bubbles mix with shallower (CO_2-poorer) conduit gas, and partially reequilibrate upon expansion, before surface discharge (*53*). (**B**) As a critical threshold is reached in the magma storage zone ($Q_s \approx Q_{ex}$), LP magma ascent starts (ascent time, 5 to 10 days) (*16*) to erupt violently on 3 July 2019. The shallow conduit undergoes fast inflation (*18*) in the last 10 min during rapid ascent (*45*, *57*) and expansion of buoyant, vesicular LP magma. (**C**) Onset of lava flow after the July 2 paroxysm progressively leads to top-down depressurization of the LP magma (during July to August 2019), ultimately triggering the 28 August 2019 paroxysm.
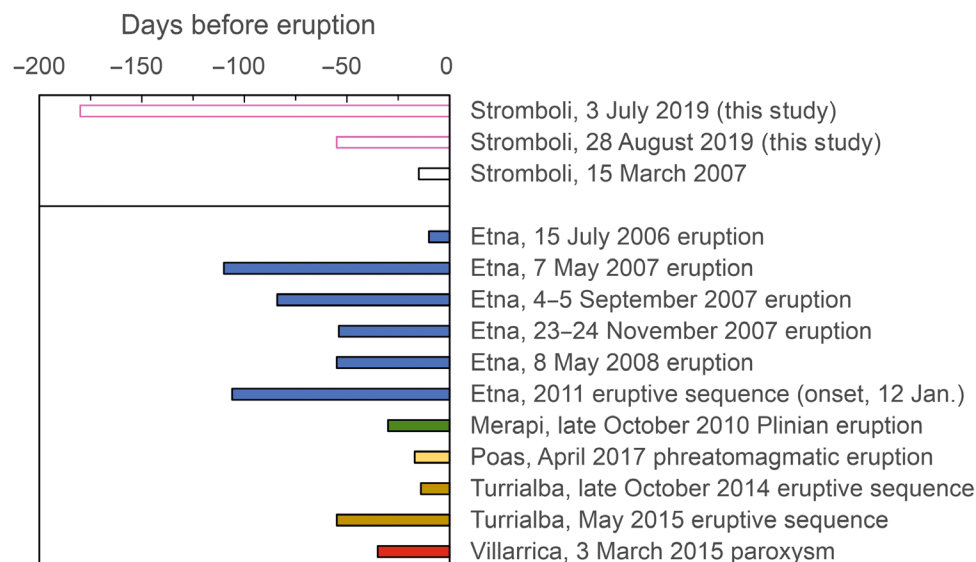
Fig. 7. Time scale of CO₂ precursors at basaltic volcanoes. The duration of the precursory plume CO_2 escalation before the July 3 and August 28 Stromboli paroxysms in 2019 compared with reported CO_2 increases before basaltic eruptions at Stromboli in 2007 (*26*) and elsewhere. Data sources: Etna (*54*), Merapi (*8*), Poás (*29*), Turrialba (*28*), and Villarrica (*27*). The pre–3 July 2019 observations extend to ~180 days the time scales over which a precursory escalation in CO_2 degassing can be resolved by instrumental gas plume monitoring. Durations of the pre–28 August 2019 and pre–15 March 2007 CO_2 precursors are significantly shorter (~56 and ~15 days, respectively) than for the 3 July 2019 event, confirming that effusions (and top-down processes in general) do accelerate unstabilization of deeply stored magma.

CO_2 supply to the LP magma storage zone may have begun up to 110 days before the blast.

Our interpretation that the anomalously high CO_2 flux before the 3 July paroxysm indicates CO_2-driven pressurization at depth requires a mechanism to promote gas transfer (decoupled from the melt) from at least 3- to 4-km depth (the minimum gas source depth, as inferred by comparing the precursory peak in CO_2/SO_2 ratio with the modeled pressure dependence of the CO_2/SO_2 ratio at Stromboli; Fig. 6A). Mineral chronometers (*16*) indicate that magma ascent only occurred within 5 to 10 days before the eruption (Fig. 6B), implying that the timing of gas transport through ascending melts is inconsistent with a several months-long CO_2 precursor if the gas and melt phases remain coupled (Figs. 4, 5, and 7). Rapid magma ascent before the blast is further supported by decompression experiments (*57*) and modeling of preblast deformation (*18*). In the context of the new emerging view of magmatic systems as complex, vertically extended plumbing systems (*58*), gas-melt decoupling and separate ascent of exsolved fluids is likely to be prevalent (*59*). Leakage of exsolved volatiles from recharged reservoirs is implicated by models (*23, 60*) and observed in analog experiments (*60*), and upward migration of magmatic fluids through permeable mush zones—such as that interconnecting the LP and HP reservoirs (Fig. 6A) (*61*)—is predicted by numerical models (*62*). At shallower levels, the relatively low viscosity of HP conduit magma allows gas to percolate through interconnected permeability until surface discharge (*63*). Ultimately, we propose that the CO_2 signal we observe captures these sequences of precursory gas leakage and decoupled ascent from a progressively overpressurizing LP magma reservoir at depth (Fig. 6A).

Top-down paroxysm's drivers

Basaltic paroxysms can also be triggered by top-down mechanisms in which eruptions are driven by shallow processes such as degassing

of conduit magma (*24*) or mass unloading by edifice (*64*) or dome (*65*) collapse, leading to decompression. Conduit unloading during effusive eruptions can also destabilize deeply stored magma; this latter process is particularly relevant for Stromboli, where the temporal association between effusion and paroxysmal activity in 2007 and 2003 has been explained by rapid decompression of the deep volcanic plumbing system by magma drainage during lava effusion (*26, 42–44*).

The 2019 effusive phase (July 3 to August 31) is the third of its kind to occur at Stromboli since the onset of volcanic CO_2 flux monitoring. It is thus useful to compare our novel CO_2 flux time series (2019) with those previously obtained in 2007 (*26*) and 2014 (*66*) to explore the possible existence of common degassing behavior. This comparison, attempted in Fig. 8, demonstrates an evident escalation in CO_2 degassing starting with the onset of the three effusive eruptions. Ultimately, the close similarity between the syn-effusive CO_2 degassing trends in 2007, 2014, and 2019 suggests a repetitive mechanism of effusion-driven perturbation of Stromboli's deep plumbing system.

On the basis of the above, we propose an effusion-driven mechanism (*26*) for the 28 August 2019 event (Figs. 5 and 6). A key observation is that, during the 2019 effusion, the break-in-slope of the cumulative CO_2 flux is delayed relative to the effusion onset (Fig. 8). Further, the SO_2 and CO_2 patterns are shifted in time (Fig. 5), with CO_2 emission (both concentrations and fluxes) increasing only when the SO_2 emission [and magma effusion rates (*67*)] reduces. We explain these observations by proposing that the 2019 effusive phase involves two phases: (i) a first period (3 July to 13 August) of rapid and efficient magma circulation in the upper conduits, characterized by high SO_2 emissions and high lava output (*67*), followed by (ii) a second period (14 to 30 August) of reduced shallow magma transport, characterized by declining SO_2 emissions and magma effusion rates concurrent with escalating deep CO_2 degassing (Fig. 5)
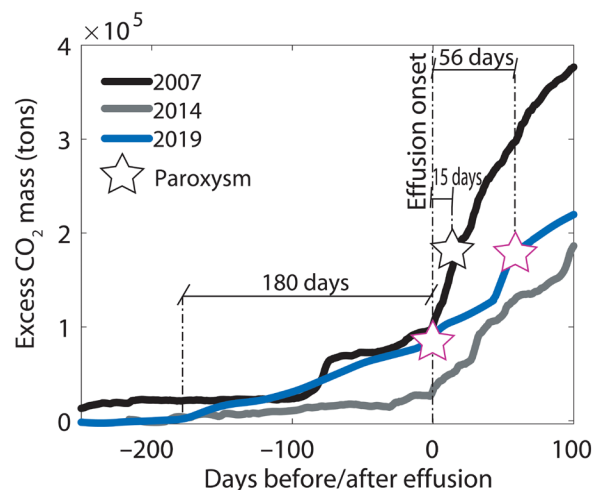
Fig. 8. CO₂ fluxes for three Stromboli's eruptions at match. Temporal record of the cumulative excess CO_2 mass at Stromboli in periods encompassing the 2007 (*26*), 2014 (*66*), and 2019 (this study) unrests. Time is expressed in days before/after effusion onset (set at 0). Excess CO_2 masses are calculated by subtracting from each CO_2 flux time series the pre-unrest averages of 650 (2007), 758 (2014), and 500 (2019) tons/day, respectively. The three paroxysms (stars) are all anticipated by visible accelerations in CO_2 release from the plume. The cumulative excess CO_2 mass ramps up since ~180 days before the eruption onset (3 July paroxysm) in 2019. The figure also demonstrates similarities in the excess CO_2 degassing trends for three effusive events (time > 0). These consistent CO_2 trends imply a systematic mechanism of effusion-driven depressurization (and degassing) of the deep plumbing system. The 2014 unrest, in which no paroxysmal explosion was observed, shows the lowest excess CO_2 masses, implying a more marginal involvement of the deep magma plumbing system.

[this study and (*67*)]. These observations are consistent with a model in which rapid drainage of conduit magma during phase 1 is the causal factor for the subsequent (phase 2) decompression, degassing, and eruption of deep magma. Again, olivine mineral chemistry in erupted pumice (*16*) evidences a deep magma pulse before the 28 August paroxysm. Overall, the degassing unrest before the 28 August 2019 paroxysm is estimated at ~56 days (Figs. 7 and 8).

We note that the 2014 effusive unrest—the only post-2000 event not associated with a paroxysmal explosion—is consistently characterized by the lowest excess CO_2 degassing budget (Fig. 8). Therefore, it appears that in 2014, the effusion had less of an impact on the deep plumbing system than in 2007 and 2019. It is possible that Stromboli's deep reservoir experienced decompression in 2014, too, but the volume of CO_2 gas involved was sufficiently low to preclude the unrest culminating into a paroxysm. Lower effusion-driven magma decompression rates in 2014 (8.4 Pa/s), relative to 2007 (29.3 Pa/s) (*43*), may have been responsible for the reduced levels of CO_2 degassing. Calculation of magma decompression rates is more complicated for the 2019 eruption as this event was not accompanied by opening of a lateral vent [that in 2003, 2007, and 2014 led to rapid lowering of magma column level in the conduit (*43*)]. However, the relatively large erupted magma volume (~6.5×10^5 m³) (*16, 67*) in only the first few (~6) hours of the effusive eruption implies fast rates of magma decompression (~30 Pa/s), sufficient to trigger the later, gradual upwelling of CO_2-rich magma finally erupted on 28 August (Fig. 5B).

Modeling the time scales of basaltic paroxysm's incubation

The duration of a paroxysm's preparation phase—i.e., the time interval between reservoir replenishment (or depressurization, for top-down mechanisms) and eruption onset—is a complex function of the geometry of the magma storage zone, magma rheology, gas bubble abundance and dimension, and gas/magma supply rate (*22, 23, 60*). However, the application of mineral chronometers at mafic volcanic systems worldwide has revealed time scales of deep magma pressurization ranging from weeks (*33*) to months (*17, 28, 34, 68–70*), similar to those determined based on erupted products from Stromboli in 2019; these similarities suggest a general process. It is therefore useful to compare the duration of the Stromboli's CO_2 precursors in 2019 to those reported before basaltic paroxysms elsewhere (Fig. 7). Through this comparison, we show that the gas precursors observed before the July 2019 event extend the time scales over which a precursory escalation in CO_2 degassing can be resolved by instrumental gas plume monitoring. Previous reports have identified elevated CO_2 emissions beginning ~15 days [Poás and Turrialba (*28–29*)] to ~50 to 100 days [Etna (*32, 54*)] before eruption (Fig. 7). In contrast, the durations of precursory signals before 28 August 2019 and 15 March 2007 paroxysms are substantially shorter (~56 and ~15 days, respectively) than those associated with the 3 July 2019 event (180 days; Figs. 7 and 8). We propose that rapid preparatory time scales may reflect the role of lava effusion (and top-down processes in general) in accelerating the destabilization of deeply stored magma (*43, 44*).

The persistent, regular activity at Stromboli has previously been interpreted in terms of a steady-state gas segregation process taking place in the HP sill-like reservoir located at ~3.5-km depth (Fig. 6A) (*60*). However, recent observations of the chemical and textural properties of erupted pyroclasts (*14–16*) indicate that Stromboli's paroxysms are fed by LP magma sourced from greater depths than the HP reservoir. We therefore apply the same gas segregation model (*60*) at conditions relevant to the ~7- to 11-km-deep LP magma reservoir (Fig. 6A).

According to the model (*60*), the time scale (T_f) to establish a steady foam layer at the roof of a sill is related to the supply rate (Q_s) of deep-derived volatile-rich magma (Fig. 6A) and to the sill size (in addition to magma rheology and gas content). It is also proposed (*60*) that the transition from regular to paroxysmal activity occurs when Q_s increases to equal the magma exchange rate Q_{ex} from the feeder conduit into the sill (e.g., when $Q_s \approx Q_{ex}$ in Fig. 6A). Under steady-state conditions, Q_{ex} is related to the outgoing gas flux (Q_g) from the foam layer into the conduit (Fig. 6A) by the expression $Q_g = cQ_{ex}$, where c is the volumetric gas fraction in the reservoir magma.

We attempt to interpret the relatively wide temporal range (from ~15 to ~180 days; Figs. 7 and 8) of the observed Stromboli's CO_2 precursors by linking them with the time scales (T_f) of foam development in the roof of the LP magma reservoir, as predicted by the model (*60*). To this aim, we rearrange equations 24 and 29 from (*60*) to establish the dependence of T_f on Q_g, the outward volumetric gas flux (in cubic meter per second) from the reservoir. This takes the form

$$T_f = \frac{L^{5/2} d^{1/2}}{k Q_g} \tag{1}$$

where L is the foam layer length (in meters; Fig. 6A), d is the bubble dimension (in meters), and k is a parameter that depends on bubble fraction ϵ in the foam and on the volumetric gas fraction c (*60*)
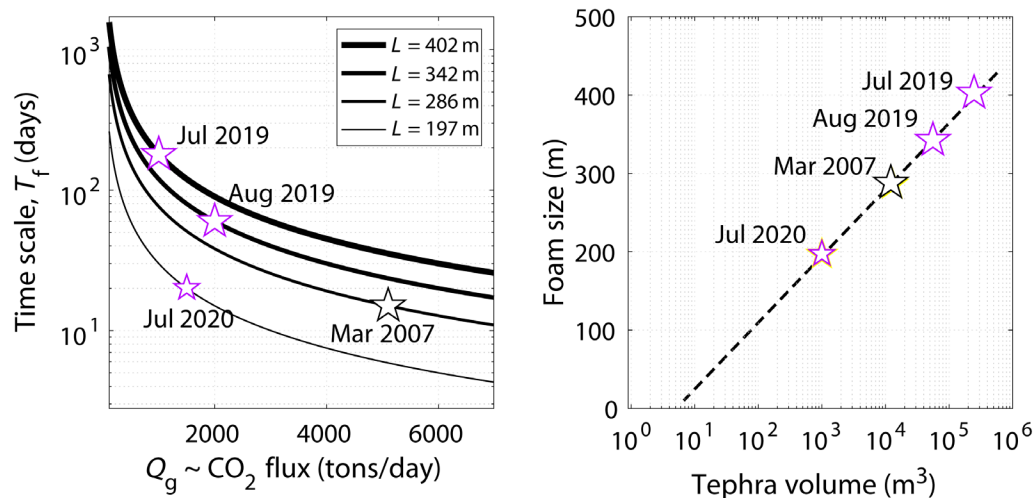
Fig. 9. Modeling the time scale of CO_2 leakage from overpressuring basaltic reservoirs. (**Left**) Time scales (T_f) of preparoxysm foam formation, calculated from using Eq. 1 [rearranged from a foam model in (60)] for a range of foam layer lengths L and gas fluxes ($Q_{g\,=\,}CO_2$ flux). For the three Stromboli paroxysms in 2007 and 2019, we use the duration of the precursory CO_2 increase (as a proxy for T_f) and mean observed preparoxysm CO_2 flux (as a proxy for Q_g). The example of the 19 July 2020 explosion (interpreted as an event intermediate in size between a small paroxysm and a large major explosion) is also illustrated. (**Right**) Scaling relationship between reservoir foam layer sizes (derived from Eq. 3) and field-derived (16) erupted LP tephra volumes. The four explosions fall along the same scaling relationship. This takes the form of an exponential correlation curve with zero intercept (deep foam layer reservoir size $L = 0$ m) for a tephra volume of ~10 m³.

$$k = \frac{\epsilon}{c}\left(\frac{c^3(1-\epsilon)^{5/2}(\epsilon-c)}{\epsilon^3}\right)^{1/4} \quad (2)$$

Equation 1 imposes that the time (T_f) required to generate a steady foam layer at the top of the reservoir is inversely proportional to Q_g. In other words, the model requires that the higher the magma exchange rate Q_{ex}, the faster the gas leakage Q_g and the shorter the time required to segregate gas in the plumbing system (a shorter T_f will also correspond to a thinner foam layer). The solutions of Eq. 1 for a range of L values, and for magma conditions relevant to Stromboli [$d = 0.1$ mm, $\epsilon = 0.7$, and $c = 0.1$ (59)], are shown in Fig. 9 (left).

In a deep magma reservoir, CO_2 dominates the gas phase (53), and Q_g will therefore correspond to the outgoing CO_2 flux from the reservoir. We therefore assume our measured mean CO_2 flux before each paroxysm approximates Q_g (e.g., the gas leakage from the reservoir), and we test whether the corresponding duration of the CO_2 flux precursor is a suitable proxy for T_f. We find that amplitudes and durations of the CO_2 flux precursors associated with the 2007 and 2019 Stromboli's paroxysms fit the model (60) well: Larger precursory fluxes are associated with shorter precursor durations (Fig. 9 left). On the basis of this match between empirical observations and model output, we propose that the rate at which CO_2 bubbles accumulate within (and leak from) a basaltic reservoir (Fig. 6) will determine the duration of a paroxysm's incubation period.

Equation 1 can also be rearranged to predict the length L of the segregated foam layer (Fig. 6A) in the LP magma reservoir as

$$L = \left(\frac{k\,T_f Q_g}{d^{1/2}}\right)^{2/5} \quad (3)$$

Using the observed precursory CO_2 fluxes (for Q_g) and durations (for T_f) in Eq. 3, we estimate foam layer length scales ranging

from ~300 m (15 March 2007 paroxysm) to ~400 m (3 July 2019) (Fig. 9 right). The estimated foam layer lengths scale well ($R^2 = 0.86$) with the independently estimated LP tephra volumes of the three explosions (16), supporting our model approach.

Testing the lower-limit resolution of gas monitoring

Paroxysmal explosions not only lie toward the upper end of a wide spectrum of eruptive intensities observed at basaltic open-vent vents volcanoes (5) but are also relatively rare. However, smaller-sized events, such as the major explosions observed at Stromboli (35, 36), also represent a substantial hazard, considering their frequent recurrence [~2 events/year on average at Stromboli (71)] and relatively large dispersal areas and impact footprint. These less voluminous events are inherently associated with smaller gas cargos (19) and, therefore, produce subtler (and more difficult to detect) gas precursors (72). Our observations, therefore, are also relevant to testing the ability of gas-monitoring networks to resolve the gas signals associated with such smaller-sized, but still very hazardous, explosions.

Seven major explosions have occurred on Stromboli during the measurement interval of this study (Figs. 2 and 4). In our record, we identify a visible CO_2 pulse in late-June to mid-July 2020, i.e., in the weeks before the 19 July 2020 explosion (Fig. 2, B and C, and Fig. 4B). Characterized by an associated ground tilt of ~3.5 μrad (measured at 750-m distance from the vents), the 19 July explosion exhibits a deformation (proportional to eruptive volumes) ~4 times higher than the average deformation associated with major explosions [0.8 μrad; based on measurement of 39 major explosions in the 2003–2020 interval (18)] but 2.5 to 4 times lower than that typically generated by paroxysms [ground tilts for the 3 July and 28 August 2019 events are 14 and 9 μrad, respectively (18)]. The 19 July 2020 explosion thus ranks at the upper range of the class of major explosions or even at the lower limit of the class of paroxysmal explosions. Clear increases above background levels observed in

CO_2 concentrations (Fig. 2B), CO_2/SO_2 ratios (Fig. 2C), and CO_2 fluxes (Fig. 4B) before the 19 July explosion support a cause-and-effect link with deep CO_2 gas. This is corroborated further by Fig. 9 (Right), in which the 19 July 2020 explosion falls on the same scaling relationship between reservoir foam size and tephra volume defined by paroxysms, implying a similar casual mechanism.

The case for smaller (than 19 July 2020) major explosions remains more complicated. In total, our record (Figs. 2 and 4) shows that six out of the seven major explosions in 2018–2020 are associated with detectable increases in CO_2/SO_2 ratios above background. However, many of these events (e.g., the three explosions in November 2020) are more challenging to resolve in the CO_2 flux record, and no detectable CO_2 signal is associated to the 18 August 2018 eruption (Figs. 2 and 4). Major explosions thus remain an enigmatic class of events. Being an order of magnitude smaller in size (*35*, *36*)—and, therefore, also in associated gas budgets (*19*)—than paroxysms, tracking a precursory CO_2 increase poses a fundamental challenge for monitoring, both at Stromboli and at other similar basaltic systems globally.

Challenges and future perspectives for gas-based monitoring of basaltic paroxysms

At open-vent volcanoes, sudden paroxysmal explosions represent a substantial threat to local populations, visitors, and scientists (*5*). These impulsive events are difficult to forecast as their source mechanisms are often rooted deep in the volcano's plumbing system. Stromboli's unrest in summer 2019, in particular, has presented a challenge for volcanologists and decision-makers. For the first time, since the volcano became instrumentally monitored, a violent paroxysmal eruption occurred (on 3 July) without a preceding phase of lava effusion, as had occurred ahead of the previous 2003 and 2007 events. Instead, the 3 July 2019 paroxysm occurred suddenly and with no obvious precursory change in surface volcanic activity, remaining unforecasted if not for a short-term (5 to 10 min before the blast) ground inflation (*18*).

A volcanic activity change may occur suddenly at basaltic volcanoes, and such an abrupt transition from regular mild Strombolian activity (and passive degassing) to paroxysmal explosions clearly highlights the limits of the current gas monitoring networks and urges on its reconsideration. If final magma ascent before a paroxysm occurs over time scales as short as few hours/days, as it seems to have been the case for the 3 July 2019 event (*16*, *57*), then the temporal resolution and continuity of our observations are fundamentally inadequate—the SO_2 flux cannot be measured during night time or when visibility is reduced, for example; and the Multi-GAS only operates a few hours per day due to power availability constraints and can retrieve useful information only when the plume fumigates the site. In addition, the 2019 eruptive crisis at Stromboli demonstrates the vulnerability of gas monitoring instrumentation that, operating in the near-vent field (<500 m from vents), are exposed to frequent damage because of exposure to harsh conditions or even to destruction during the explosions.

Ultimately, the lesson learned from the 2019 eruptive crisis is that the extremely rapid (days) final magma ascent before paroxysmal activity requires the acquisition of robust, continuous, and high-temporal resolution gas records and real-time data analysis. The lack of data continuity in the months before the 3 July 2019 event hindered recognition and interpretation of the observed CO_2 peak (which remained unreported at that time), thereby demonstrating

the limitations of current gas monitoring technologies. This, notwithstanding the time series of gas composition and flux at Stromboli, remains among the longest and most continuous on record for an active volcano. If detecting short-term (minutes/hours) preblast changes appear challenged by the inadequate temporal resolution, then the fact that the paroxysm preparatory phase can occur over time scales as long as months, as our data suggest, provides additional confidence in volcanic gas monitoring infrastructure. Ultimately, we propose that the persistence (for weeks/months) of heightened CO_2 emissions marks a critical condition in which the deep plumbing system has become unstable and prone to eruption. Thus, our volcanic gas observations bring new general implications for tracking the preparation periods of these hazardous explosive eruptions and confirm the utility of in situ CO_2 monitoring. Our results also urge the development of novel and complementary imaging techniques that allow the volcanic CO_2 flux to be remotely observed in real time from "safer" distal locations.

MATERIALS AND METHODS
Experimental design
The volcanic gas results we report in this study are based on an integrated instrumental network for fully automated, real-time volcanic gas observations. The network is in operation on Stromboli since 2014 (Fig. 1).

Gas composition
Our volcanic gas composition dataset is based on in situ measurements of in-plume CO_2 and SO_2 concentrations (Fig. 2) using Multi-GAS, deployed in the Pizzo Sopra la Fossa area (Fig. 1D). Our Multi-GAS, assembled at Dipartimento di Scienze della Terra e del Mare (DiSTeM) [Università di Palermo (UniPa)], uses a Campbell CR6 data logger to command operations of an infrared spectrometer (model Gascard NG from Edinburgh Sensors; 0 to 3000 ppmv of calibration range, accuracy of ±1.5%, and resolution of 0.1 ppmv) to measure in-plume CO_2 and a specific electrochemical sensor to measure in-plume SO_2 (model SO_2 T3ST/F-TD2G-1A from City Technology; 0 to 200 ppmv of calibration range, accuracy of ±2%, and resolution of 0.1 ppmv). Signals from both sensors are simultaneously captured by the data logger at 0.5- to 1-Hz rate during sequences of operation cycles. Duration and daily number of measurement cycles vary day by day. The system is configured to automatically activate every 1 to 4 hours (depending on power availability) and to check the SO_2 concentration levels for ~300 s, after which the measurement cycle is aborted (and the instrument enters a sleep mode) if SO_2 concentrations are below the 1-ppmv threshold. Otherwise, the Multi-GAS remains in operational mode (signals acquired and stored in the data logger memory card) for 30 min. Data are then transmitted (using a Ubiquiti NanoStation 5GHz antenna, model NSM5) back to the Centro Operativo Avanzato (COA, Stromboli; Fig. 1D, inset) and then transferred to DiSTeM.

We back-process the entire dataset using a novel algorithm that sequentially explores the CO_2 and SO_2 concentration time series using a 60-s-long moving window (scanning data acquired during each acquisition cycle). Tests made indicate that a 60-s window corresponds to the best compromise between the need of high temporal resolution and the necessity of having a sufficient number of CO_2 and SO_2 concentration couples (30 and 60 for 0.5- and 1-Hz acquisition frequencies, respectively). This new processing differs

from previous Multi-GAS work on Stromboli (26, 53) in that species concentrations are evaluated focusing on their maximum concentration differences within the analyzed window (Fig. 3) rather than on their maximum absolute values. This procedure allows minimizing, especially for CO_2, the atmospheric contribution to the measured signals, emphasizing the differential contribution due to transient plume arrivals (Fig. 3) at the measurement point. Ultimately, this allows us to expand the processed signal range down to the acquisition threshold of 1-ppmv SO_2 [previous work has relied on filtered data subsets with SO_2 above a 4- to 5-ppmv threshold (26, 53)]. Within each scanned 60-s-long temporal interval, the routine searches for any temporal coherence between the CO_2 and SO_2 concentration time series (Fig. 3). We set a Pearson correlation coefficient threshold at ≥0.9, and we only consider intervals in which (i) this correlation threshold is achieved and (ii) the SO_2 concentration range (maximum to minimum) is ≥1 ppm. Tests made using different thresholds (≥0.5 ppm) produce similar results, but we conservatively use a ≥1-ppm threshold throughout. For SO_2 oscillations (within a 60-s interval) of <0.5 ppm, the CO_2 versus SO_2 correlations become increasingly poor. For any successful interval (in which both thresholds are achieved), the algorithm outputs the SO_2 and CO_2 concentration levels (illustrated in Fig. 2, A and B, respectively) and the corresponding CO_2/SO_2 molar ratio. The latter is obtained from the first-order coefficient of the best-fit linear regression function calculated from CO_2 and SO_2 concentration time series within the processing window (Fig. 3). The derived CO_2/SO_2 molar ratios are illustrated in Fig. 2C. The entire dataset is provided as data S1.

UV camera–derived SO_2 fluxes

To convert the derived plume CO_2/SO_2 ratios into volcanic CO_2 fluxes (Fig. 4B), we take advantage of SO_2 fluxes (see Fig. 4A) obtained from the processing of images delivered by a permanent, fully autonomous dual UV camera system. This UV camera (also assembled at DiSTeM) is installed on the volcano summit, at about ~500-m distance from the active craters (UV1; Fig. 1D), and is designed to automatically acquire (at 0.5-Hz rate) and process sets of images, acquired during 6-hour-long daily acquisition cycles. Measurement principles of the UV (or SO_2) camera are detailed elsewhere (73, 74), while hardware, software, and acquisition/processing routines are described in (75, 76). The system is equipped with two JAI CM-140GE-UV cameras sensible to UV radiation and is fitted with two distinct band-pass optical filters (both with 10 nm of full width at half maximum) with central wavelengths of 310 nm (SO_2 absorption) and 330 nm (no SO_2 absorption). A collocated spectrometer (Ocean-Optic USB2000+) is used to calibrate the UV camera images (75, 76), in addition to periodic calibration campaigns with gas cells of known SO_2 concentration.

The crater terrace's geometry determines the fraction of the crater plume that can be imaged (and resolved) by the camera. The UV1 camera system is deployed at the Roccette site (38°47′53″ N, 15°13′0.1″ E; northeast upper flank of Stromboli, at 750 m a.s.l. (above sea level); see Fig. 1D) and is operative since June 2014 (58). Given its positioning, this system can adequately resolve the SO_2 flux emissions from the North-East (NEC) and Central (CC) craters (52, 77), while it severely underestimates emissions from the South-West (SWC) crater (that is hidden by the NEC ridge) (Fig. 1D). This underestimation is confirmed by the fact that our UV camera–derived SO_2 fluxes are systematically lower than those delivered by

the FLAME (FLux Automatic MEasurements) network of scanning spectrometers (51) operated by INGV-OE (Istituto Nazionale di Geofisica e Vulcanologia, Osservatorio Etneo, Catania; see recent datasets available in internal reports at www.ct.ingv.it) that sense the bulk, more distal plume. Experiments made during 2017–2019 using, simultaneously, a second UV camera system, positioned on the Stromboli's upper southwest flank, indicate that the UV1 camera system underestimate the volcano's total SO_2 emissions by a factor ~48% on average, and we use this correction factor to (at least partially) account for the SO_2 fraction "unseen" by UV1.

Given the short proximity of the UV camera from the target plume and the small error (±5%) associated with plume transport speed measurements [derived by tracking the motion of plume gas fronts using an optical flow algorithm (76)], we estimate SO_2 flux uncertainty to be dominated by errors in radiative transfer. This corresponds to ~±30% (74) at the low SO_2/ash in-plume contents observed at Stromboli. The entire dataset is provided as data S2.

CO_2 fluxes

Our reported CO_2 fluxes (Figs. 4B and 5) are derived by multiplying the daily CO_2/SO_2 ratio frequency diagrams (shown in Fig. 2C) by the daily averaged SO_2 fluxes (Fig. 4A and data S2). Uncertainty in the derived CO_2 fluxes is evaluated at ≤40% from propagation of CO_2/SO_2 and SO_2 flux uncertainties. The daily median CO_2 fluxes, corresponding to the dominant CO_2 flux values (dark red tones in the normalized frequency distribution diagrams of Fig. 4B), are listed in data S3.

REFERENCES AND NOTES

1. B. F. Houghton, H. M. Gonnermann, Basaltic explosive volcanism: Constraints from deposits and models. *Chemie der Erde* **68**, 117–140 (2008).
2. C. M. Allison, K. Roggensack, A. B. Clarke, Highly explosive basaltic eruptions driven by CO_2 exsolution. *Nat. Commun.* **12**, 217 (2021).
3. M. Coltelli, P. Del Carlo, L. Vezzoli, Discovery of a Plinian basaltic eruption of Roman age at Etna volcano, Italy. *Geology* **26**, 1095–1098 (1998).
4. L. Costantini, C. Bonadonna, B. F. Houghton, H. Wehrmann, New physical characterization of the Fontana Lapilli basaltic Plinian eruption, Nicaragua. *Bull. Volcanol.* **71**, 337 (2009).
5. W. I. Rose, J. L. Palma, H. Delgado Granados, N. Varley, Understanding open-vent volcanism and related hazard. *Geol. Soc. Am. Special Papers* **498**, 10.1130/SPE498, (2013).
6. J. Battaglia, S. Hidalgo, B. Bernard, A. Steele, S. Arellano, K. Acuña, Autopsy of an eruptive phase of Tungurahua volcano (Ecuador) through coupling of seismo-acoustic and SO_2 recordings with ash characteristics. *Earth Planet. Sci. Lett.* **511**, 223–232 (2019).
7. A. K. Naismith, I. M. Watson, R. Escobar-Wolf, G. Chigna, H. Thomas, D. Coppola, C. Chun, Eruption frequency patterns through time for the current (1999–2018) activity cycle at Volcán de Fuego derived from remote sensing data: Evidence for an accelerating cycle of explosive paroxysms and potential implications of eruptive activity. *J. Volcanol. Geotherm. Res.* **371**, 206–219 (2019).
8. Surono, P. Jousset, J. Pallister, M. Boichu, M. Fabrizia Buongiorno, A. Budisantoso, F. Costa, S. Andreastuti, F. Prata, D. Schneider, L. Clarisse, H. Humaida, S. Sumarti, C. Bignami, J. Griswold, S. Carn, C. Oppenheimer, F. Lavigne, The 2010 explosive eruption of Java's Merapi volcano—A '100-year' event. *J. Volcanol. Geotherm. Res.* **241–242**, 121–135 (2012).
9. F. Arzilli, G. La Spina, M. R. Burton, M. Polacci, N. Le Gall, M. E. Hartley, D. Di Genova, B. Cai, N. T. Vo, E. C. Bamber, S. Nonni, R. Atwood, E. W. Llewellin, R. A. Brooker, H. M. Mader, P. D. Lee, Magma fragmentation in highly explosive basaltic eruptions induced by rapid crystallization. *Nat. Geosci.* **12**, 1023–1028 (2019).
10. G. La Spina, F. Arzilli, E. W. Llewellin, M. R. Burton, A. B. Clarke, M. de Michieli Vitturi, M. Polacci, M. E. Hartley, D. Di Genova, H. M. Mader, Explosivity of basaltic lava fountains is controlled by magma rheology, ascent rate and outgassing. *Earth Planet. Sci. Lett.* **553**, 116658 (2021).
11. H. M. Gonnermann, Magma fragmentation. *Annu. Rev. Earth Planet. Sci.* **43**, 431–458 (2015).

12. National Academies of Sciences, Engineering, and Medicine, *Volcanic Eruptions and Their Repose, Unrest, Precursors, and Timing* (The National Academies Press, 2017).

13. M. Cassidy, M. Manga, K. Cashman, O. Bachmann, Controls on explosive-effusive volcanic eruption styles. *Nat. Commun.* **9**, 2839 (2018).

14. N. Métrich, A. Bertagnini, P. Landi, M. Rosi, O. Belhadj, Triggering mechanism at the origin of paroxysms at Stromboli (Aeolian archipelago, Italy): The 5 April 2003 eruption. *Geophys. Res. Lett.* **32**, L10305 (2005).

15. N. Métrich, A. Bertagnini, A. Di Muro, Conditions of magma storage, degassing and ascent at Stromboli: New insights into the volcano plumbing system with inferences on the eruptive dynamics. *J. Petrol.* **51**, 603–626 (2010).

16. N. Métrich, A. Bertagnini, M. Pistolesi, Paroxysms at Stromboli volcano (Italy): Source, genesis and dynamics. *Front. Earth Sci.* **9**, 593339 (2021).

17. F. Costa, S. Andreastuti, C. Bouvet de Maisonneuve, J. S. Pallister, Petrological insights into the storage conditions, and magmatic processes that yielded the centennial 2010 Merapi explosive eruption. *J. Volcanol. Geotherm. Res.* **261**, 209–235 (2013).

18. M. Ripepe, G. Lacanna, M. Pistolesi, M. C. Silengo, A. Aiuppa, M. Laiolo, F. Massimetti, L. Innocenti, M. Della Schiava, M. Bitetto, F. P. La Monica, T. Nishimura, M. Rosi, D. Mangione, A. Ricciardi, R. Genco, D. Coppola, E. Marchetti, D. Delle Donne, Ground deformation reveals the scale-invariant conduit dynamics driving explosive basaltic eruptions. *Nat. Commun.* **12**, 1683 (2021).

19. P. Allard, A CO_2-rich gas trigger of explosive paroxysms at Stromboli basaltic volcano, Italy. *J. Volcanol. Geotherm. Res.* **189**, 363–374 (2010).

20. J. Blundy, K. V. Cashman, A. Rust, F. Witham, A case for CO_2-rich arc magmas. *Earth Planet. Sci. Lett.* **290**, 289–301 (2010).

21. A. Aiuppa, R. Moretti, C. Federico, G. Giudice, S. Gurrieri, M. Liuzzo, P. Papale, H. Shinohara, M. Valenza, Forecasting Etna eruptions by real-time observation of volcanic gas composition. *Geology* **35**, 1115–1118 (2007).

22. A. W. Woods, S. S. S. Cardoso, Triggering basaltic volcanic eruptions by bubble-melt separation. *Nature* **385**, 518–520 (1997).

23. J. C. Phillips, A. W. Woods, Bubble plumes generated during recharge of basaltic magma reservoirs. *Earth Planet. Sci. Lett.* **186**, 297–309 (2001).

24. T. Girona, F. Costa, G. Schubert, Degassing during quiescence as a trigger of magma ascent and volcanic eruptions. *Sci. Rep.* **5**, 18212 (2015).

25. C. Werner, T. P. Fischer, A. Aiuppa, M. Edmonds, C. Cardellini, S. Carn, G. Chiodini, E. Cottrell, M. Burton, H. Shinohara, P. Allard, Carbon dioxide emissions from subaerial volcanic regions: Two decades in review, in *Deep Carbon Past to Present*, B. N. Orcutt, I. Daniel, R. Dasgupta, Eds. (Cambridge Univ. Press, 2019), chap. 8, pp. 188–236.

26. A. Aiuppa, M. Burton, T. Caltabiano, G. Giudice, S. Guerrieri, M. Liuzzo, F. Murè, G. Salerno, Unusually large magmatic CO_2 gas emissions prior to a basaltic paroxysm. *Geophys. Res. Lett.* **37**, L17303 (2010).

27. A. Aiuppa, M. Bitetto, V. Francofonte, G. Velasquez, C. B. Parra, G. Giudice, M. Liuzzo, R. Moretti, Y. Moussallam, N. Peters, G. Tamburello, O. A. Valderrama, A. Curtis, A CO_2-gas precursor to the March 2015 Villarrica volcano eruption. *Geochem. Geophys. Geosys.* **18**, 2120–2132 (2017).

28. J. M. de Moor, A. Aiuppa, G. Avard, H. Wehrmann, N. W. Dunbar, C. Muller, G. Tamburello, G. Giudice, M. Liuzzo, R. Moretti, V. Conde, B. Galle, Turmoil at Turrialba Volcano (Costa Rica): Degassing and eruptive processes inferred from high-frequency gas monitoring. *J. Geophys. Res. Solid Earth* **121**, 5761–5775 (2016).

29. J. M. de Moor, J. Stix, G. Avard, C. Muller, E. Corrales, J. A. Diaz, A. Alan, J. Brenes, J. Pacheco, A. Aiuppa, T. P. Fischer, Insights on hydrothermal-magmatic interactions and eruptive processes at Poás volcano (Costa Rica) from high-frequency gas monitoring and drone measurements. *Geophys. Res. Lett.* **46**, 1293–1302 (2019).

30. M. R. Burton, P. Allard, F. Muré, A. La Spina, Magmatic gas composition reveals the source depth of slug-driven strombolian explosive activity. *Science* **37**, 227–230 (2007).

31. P. Allard, M. Burton, F. Murè, Spectroscopic evidence for a lava fountain driven by previously accumulated magmatic gas. *Nature* **433**, 407–410 (2005).

32. D. Patanè, A. Aiuppa, M. Aloisi, B. Behncke, A. Cannata, M. Coltelli, G. di Grazia, S. Gambino, S. Gurrieri, M. Mattia, G. Salerno, Insights into magma and fluid transfer at Mount Etna by a multiparametric approach: A model of the events leading to the 2011 eruptive cycle. *J. Geophys. Res. Solid Earth* **118**, 3519–3539 (2013).

33. T. Ubide, B. S. Kamber, Volcanic crystals as time capsules of eruption history. *Nat. Commun.* **9**, 326 (2018).

34. F. Costa, R. Dohmen, S. Chakraborty, Time scales of magmatic processes from modeling the zoning patterns of crystals. *Rev. Mineralogy Geochem.* **69**, 545–594 (2008).

35. L. Pioli, M. Pistolesi, M. Rosi, Transient explosions at open-vent volcanoes: The case of Stromboli (Italy). *Geology* **42**, 863–866 (2014).

36. M. Rosi, M. Pistolesi, A. Bertagnini, P. Landi, M. Pompilio, A. Di Roberto, Stromboli volcano, Aeolian Islands (Italy): Present eruptive activity and hazards, in *The Aeolian Islands Volcanoes*, F. Lucchi, A. Peccerillo, J. Keller, C. A. Tranne, P. L. Rossi, Eds. (*Geol. Soc. Lon. Mem.*, 2013), vol. 37, pp. 475–492.

37. A. Bertagnini, A. Di Roberto, M. Pompilio, Paroxysmal activity at Stromboli: Lessons from the past. *Bull. Volc.* **73**, 1229–1243 (2011).

38. S. Calvari, L. Spampinato, L. Lodato, The 5 April 2003 Vulcanian paroxysmal explosion at Stromboli volcano (Italy) from field observations and thermal data. *J. Volcanol. Geotherm. Res.* **149**, 160–175 (2006).

39. M. Rosi, A. Bertagnini, A. J. L. Harris, L. Pioli, M. Pistolesi, M. Ripepe, A case history of paroxysmal explosion at Stromboli: Timing and dynamics of the April 5, 2003 event. *Earth Planet. Sci. Lett.* **243**, 594–606 (2006).

40. M. Pistolesi, D. Delle Donne, L. Pioli, M. Rosi, M. Ripepe, The 15 March 2007 explosive crisis at Stromboli volcano, Italy: Assessing physical parameters through a multidisciplinary approach. *J. Geophys. Res.* **116**, B12206 (2011).

41. N. Métrich, A. Bertagnini, P. Landi, M. Rosi, Crystallization driven by decompression and water loss at Stromboli volcano (Aeolian Islands, Italy). *J. Petrol.* **42**, 1471–1490 (2001).

42. S. Calvari, L. Spampinato, A. Bonaccorso, C. Oppenheimer, E. Rivalta, E. Boschi, Lava effusion—A slow fuse for paroxysms at Stromboli volcano? *Earth Planet. Sci. Lett.* **301**, 317–323 (2011).

43. M. Ripepe, M. Pistolesi, D. Coppola, D. Delle Donne, R. Genco, G. Lacanna, M. Laiolo, E. Marchetti, G. Ulivieri, S. Valade, Forecasting effusive dynamics and decompression rates by magmastatic model at open-vent volcanoes. *Sci. Rep.* **7**, 3885 (2017).

44. M. Ripepe, D. Delle Donne, R. Genco, G. Maggio, M. Pistolesi, E. Marchetti, P. Poggi, Volcano seismicity and ground deformation unveil the gravity-driven magma discharge dynamics of a volcanic eruption. *Nat. Commun.* **6**, 6998 (2015).

45. N. Le Gall, M. Pichavant, Effect of ascent rate on homogeneous bubble nucleation in the system basalt-H_2O-CO_2: Implications for Stromboli volcano. *Am. Mineral.* **101**, 1967–1985 (2016).

46. G. Giordano, G. De Astis, The summer 2019 basaltic Vulcanian eruptions (paroxysms) of Stromboli. *Bull. Volcanol.* **83**, 1 (2021).

47. F. Giudicepietro, C. López, G. Macedonio, S. Alparone, F. Bianco, S. Calvari, W. De Cesare, D. Delle Donne, B. Di Lieto, A. M. Esposito, M. Orazi, R. Peluso, E. Privitera, P. Romano, G. Scarpato, A. Tramelli, Geophysical precursors of the July-August 2019 paroxysmal eruptive phase and their implications for Stromboli volcano (Italy) monitoring. *Sci. Rep.* **10**, 10296 (2020).

48. G. Lacanna, M. Ripepe, Genesis of tsunami waves generated by Pyroclastic flows and the Early-Warning system, in 4th Rittmann conference Abstract volume (Miscellanea INGV, **52**, 2020), Catania, 12 to 14 February 2020.

49. G. Chiodini, F. Giudicepietro, J. Vandemeulebrouck, A. Aiuppa, S. Caliro, W. De Cesare, G. Tamburello, R. Avino, M. Orazi, L. D'Auria, Fumarolic tremor and geochemical signals during a volcanic unrest. *Geology* **45**, 1131–1134 (2017).

50. G. Tamburello, S. Caliro, G. Chiodini, P. De Martino, R. Avino, C. Minopoli, A. Carandente, D. Rouwet, A. Aiuppa, A. Costa, M. Bitetto, G. Giudice, V. Francofonte, T. Ricci, A. Sciarra, E. Bagnato, F. Capecchiacci, Escalating CO_2 degassing at the Pisciarelli fumarolic system, and implications for the ongoing Campi Flegrei unrest. *J. Volcanol. Geotherm. Res.* **384**, 151–157 (2019).

51. M. Burton, T. Caltabiano, F. Murè, G. Salerno, D. Randazzo, SO_2 flux from Stromboli during the 2007 eruption: Results from the FLAME network and traverse measurements. *J. Volcanol. Geotherm. Res.* **182**, 214–220 (2009).

52. D. Delle Donne, G. Tamburello, A. Aiuppa, M. Bitetto, G. Lacanna, R. D'Aleo, M. Ripepe, Exploring the explosive-effusive transition using permanent ultraviolet cameras. *J. Geophys. Res. Solid Earth* **122**, 4377–4394 (2017).

53. A. Aiuppa, A. Bertagnini, N. Métrich, R. Moretti, A. Di Muro, M. Liuzzo, G. Tamburello, A model of degassing for Stromboli volcano. *Earth Planet. Sci. Lett.* **295**, 195–204 (2010).

54. A. Aiuppa, G. Giudice, M. Liuzzo, Volcanic gas plume data from Etna Volcano (Italy), Version 1.0, in *Interdisciplinary Earth Data Alliance* (IEDA, 2017); https://doi.org/10.1594/IEDA/100643.

55. E. J. Liu, K. V. Cashman, E. Miller, H. Moore, M. Edmonds, B. E. Kunz, F. Jenner, G. Chigna, Petrologic monitoring at Volcán de Fuego, Guatemala. *J. Volcanol. Geotherm. Res.* **405**, 107044 (2020).

56. S. Inguaggiato, F. Vita, M. Cangemi, L. Calderone, Changes in CO_2 soil degassing style as a possible precursor to volcanic activity: The 2019 case of Stromboli paroxysmal eruptions. *Appl. Sci.* **10**, 4757 (2020).

57. M. Pichavant, I. Di Carlo, M. Pompilio, N. Le Gall, Experimental simulation of ascent and fragmentation of Stromboli LP magmas, in 4th Rittmann conference Abstract volume (Miscellanea INGV, **52**, 2020), Catania, 12 to 14 February 2020.

58. K. V. Cashman, R. S. J. Sparks, J. D. Blundy, Vertically extensive and unstable magmatic systems: A unified view of igneous processes. *Science* **355**, eaag3055 (2017).

59. T. E. Christopher, J. Blundy, K. Cashman, P. Cole, M. Edmonds, P. J. Smith, R. S. J. Sparks, A. Stinton, Crustal-scale degassing due to magma system destabilization and magma-gas decoupling at Soufrière Hills Volcano, Montserrat. *Geochem. Geophys. Geosyst.* **16**, 2797–2811 (2015).

60. T. Menand, J. C. Phillips, Gas segregation in dykes and sills. *J. Volcanol. Geotherm. Res.* **159**, 393–408 (2007).

61. L. Francalanci, R. Avanzinelli, I. Nardini, M. Tiepolo, J. P. Davidson, R. Vannucci, Crystal recycling in the steady-state system of the active Stromboli volcano: A 2.5-ka story inferred from in situ Sr-isotope and trace element data. *Contrib. Mineral. Petrol.* **163**, 109–131 (2012).

62. O. Bachmann, G. W. Bergantz, Gas percolation in upper-crustal silicic crystal mushes as a mechanism for upward heat advection and rejuvenation of near-solidus magma bodies. *J. Volcanol. Geotherm. Res.* **149**, 85–102 (2006).

63. M. R. Burton, H. M. Mader, M. Polacci, The role of gas percolation in quiescent degassing of persistently active basaltic volcanoes. *Earth Planet. Sci. Lett.* **264**, 46–60 (2007).

64. T. R. Walter, M. Haghshenas Haghighi, F. M. Schneider, D. Coppola, M. Motagh, J. Saul, A. Babeyko, T. Dahm, V. R. Troll, F. Tilmann, S. Heimann, S. Valade, R. Triyono, R. Khomarudin, N. Kartadinata, M. Laiolo, F. Massimetti, P. Gaebler, Complex hazard cascade culminating in the Anak Krakatau sector collapse. *Nat. Commun.* **10**, 4339 (2019).

65. B. Voight, A. T. Linde, I. S. Sacks, G. S. Mattioli, R. S. J. Sparks, D. Elsworth, D. Hidayat, P. E. Malin, E. Shalev, C. Widiwijayanti, S. R. Young, V. Bass, A. Clarke, P. Dunkley, W. Johnston, N. McWhorter, J. Neuberg, P. Williams, Unprecedented pressure increase in deep magma reservoir triggered by lava-dome collapse. *Geophys. Res. Lett.* **33**, L03312 (2006).

66. M. Liuzzo, A. Aiuppa, G. Salerno, M. Burton, C. Federico, T Caltabiano, G. Giudice, G. Giuffrida, The 2007 and 2014 eruptions of Stromboli at match: Monitoring the potential occurrence of effusion-driven basaltic paroxysmal explosions from a volcanic CO_2 flux perspective, in *Geophysical Research Abstracts* **17**, EGU2015-8715 (2015 EGU General Assembly 2015, 2015).

67. M. Laiolo, D. Coppola, F. Massimetti, C. Cigolini, M. Della Schiava, L. Innocenti, G. Lacanna, F. La Monica, E. Marchetti, M. C. Silengo, M. Ripepe, A. Aiuppa, M. Bitetto, D. Delle Donne, M. Pistolesi, The 2019 Stromboli eruptive crisis monitored from space: Insights on thermal activity, effusion rates and erupted volume, in *4th Rittmann conference Abstract volume (Miscellanea INGV, **52**, 2020)*, Catania, 12 to 14 February 2020.

68. M. Kahl, S. Chakraborty, F. Costa, M. Pompilio, Dynamic plumbing system beneath volcanoes revealed by kinetic modeling, and the connection to monitoring data: An example from Mt. Etna. *Earth Planet. Sci. Lett.* **308**, 11–22 (2011).

69. D. J. Morgan, S. Blake, N. W. Rogers, B. DeVivo, G. Rolandi, R. Macdonald, C. J. Hawkesworth, Time scales of crystal residence and magma chamber volume from modelling of diffusion profiles in phenocrysts: Vesuvius 1944. *Earth Planet. Sci. Lett.* **222**, 933–946 (2004).

70. C. Bouvet de Maisonneuve, F. Costa, C. Huber, P. Vonlanthen, O. Bachmann, M. A. Dungan, How do olivines record magmatic events? Insights from major and trace element zoning. *Contrib. Mineral. Petrol.* **171**, 56 (2016).

71. A. Bevilacqua, A. Bertagnini, M. Pompilio, P. Landi, P. Del Carlo, A. Di Roberto, W. Aspinall, A. Neri, Major explosions and paroxysms at Stromboli (Italy): A new historical catalog and temporal models of occurrence with uncertainty quantification. *Sci. Rep.* **10**, 17357 (2020).

72. A. Aiuppa, M. Burton, P. Allard, T. Caltabiano, G. Giudice, S. Gurrieri, M. Liuzzo, G. Salerno, First observational evidence for the CO_2-driven origin of Stromboli's major explosions. *Solid Earth* **2**, 135–142 (2011).

73. T. Mori, M. R. Burton, The SO_2 camera: A simple, fast and cheap method for ground-based imaging of SO_2 in volcanic plumes. *Geophys. Res. Lett.* **33**, L24804 (2006).

74. C. Kern, F. Kick, P. Lübcke, L. Vogel, M. Wöhrbach, U. Platt, Theoretical description of functionality, applications, and limitations of SO_2 cameras for the remote sensing of volcanic plumes. *Atmos. Meas. Tech.* **3**, 733–749 (2010).

75. D. Delle Donne, M. Ripepe, G. Lacanna, G. Tamburello, M. Bitetto, A. Aiuppa, Gas mass derived by infrasound and UV cameras: Implications for mass flow rate. *J. Volcanol. Geotherm. Res.* **325**, 169–178 (2016).

76. D. Delle Donne, A. Aiuppa, M. Bitetto, R. D'Aleo, M. Coltelli, D. Coppola, E. Pecora, M. Ripepe, G. Tamburello, Changes in SO_2 flux regime at Mt. Etna captured by automatically processed ultraviolet camera data. *Remote Sens. (Basel)* **11**, 1201 (2019).

77. T. D. Pering, E. J. Liu, K. Wood, T. C. Wilkes, A. Aiuppa, G. Tamburello, M. Bitetto, T. Richardson, A. J. S. McGonigle, Combined ground and aerial measurements resolve vent-specific gas fluxes from a multi-vent volcano. *Nat. Commun.* **11**, 3039 (2020).

Science Advances

Volcanic CO tracks the incubation period of basaltic paroxysms

Alessandro AiuppaMarcello BitettoDario Delle DonneFrancesco Paolo La MonicaGiancarlo TamburelloDiego CoppolaMassimo Della SchiavaLorenzo InnocentiGiorgio LacannaMarco LaioloFrancesco MassimettiMarco PistolesiMaria Cristina SilengoMaurizio Ripepe

View the article online
https://www.science.org/doi/10.1126/sciadv.abh0191
Permissions
https://www.science.org/help/reprints-and-permissions

Use of think article is subject to the Terms of service